Solid-phase growth mechanism of tungsten oxide nanowires synthesized on sputtered tungsten film

Y. Kojima[a),b)]
Department of Engineering Synthesis, School of Engineering, The University of Tokyo, 7-3-1 Hongo, Bunkyo-ku, Tokyo 113-8656, Japan

K. Kasuya
Central Research Laboratory, Hitachi, Ltd., I-280 Higashi-koigakubo, Kokubunji, Tokyo 185-8601, Japan

K. Nagato[a),c)]
Department of Engineering Synthesis, School of Engineering, The University of Tokyo, 7-3-1 Hongo, Bunkyo-ku, Tokyo 113-8656, Japan and Research Fellow of the Japan Society for the Promotion of Science, 8 Ichibancho, Chiyoda-ku, Tokyo 102-8472, Japan

T. Hamaguchi and M. Nakao
Department of Engineering Synthesis, School of Engineering, The University of Tokyo, 7-3-1 Hongo, Bunkyo-ku, Tokyo 113-8656, Japan

(Received 21 April 2008; accepted 2 September 2008; published 18 November 2008)

The authors have proposed a solid-phase growth mechanism of tungsten oxide nanowires synthesized on sputtered tungsten films. Transmission electron microscopy observation, x-ray diffraction analyses, and some *ex situ* experiments were performed to verify the growth model. The nanowire nuclei are generated at irregular points on the W surface. An amorphous oxidized layer is formed on the W surface by annealing, and tungsten oxide molecules migrate on the W surface into the nuclei, thus contributing to the nanowire growth. © *2008 American Vacuum Society.*
[DOI: 10.1116/1.2990783]

I. INTRODUCTION

Tungsten oxide nanowires are synthesized by the simple annealing of tungsten materials such as tungsten foils,[1] wires,[2–4] filaments,[5–10] sputtered films,[11–15] powders,[16–24] or tips.[25,26] The nanowires are one-dimensional nanostructures that have diameters of 10–100 nm and lengths of 100–1000 nm. The nanowires have attracted much attention as promising materials for field emitters,[13,18,24,26–29] gas sensors,[17] and electrochromic devices[19] because they have unique electric and chemical properties and high aspect ratios. Many studies have reported various growth mechanisms of the nanowires. Vapor-solid (V-S) growth has been proposed,[1–3,5–9,11,16,21,24,25,27,30] in which the nanowires grow when tungsten oxide molecules, which evaporate by annealing, are absorbed on the material. V-S growth was suggested on the basis that nanowires were synthesized on the substrate away from the tungsten material.[1,2,5–8,16,24,27] Solid-phase growth[4,12,22,31–33] has also been proposed, in which the nanowires grow when tungsten oxide molecules migrate on the surface or in the material without being evaporated, and then contribute to nanowire growth from the root.

Our group has synthesized nanowires using sputtered films as tungsten material.[13–15] Sputtered films are patternable, and this method is favorable for the fabrication of devices containing nanowires. For the growth mechanism of nanowires synthesized on sputtered films, both V-S growth[12] and solid-phase growth[11] have been proposed, and a convincing growth model has not been established to date.

In this article, we propose that solid-phase growth is the growth mechanism of the nanowires synthesized on the sputtered film. We suggest this model from the results of transmission electron microscopy (TEM) observations and x-ray diffraction (XRD) analyses of the tungsten film and the nanowires in three stages: before the nanowire synthesis, at the initial stage of nanowire growth, and after nanowire growth. Furthermore, we verify the proposed growth model by performing some *ex situ* experiments.

II. TEM OBSERVATIONS AND XRD ANALYSES

A. Preparation of samples

We used sputtered W/Cr films on Si substrates with thicknesses of 200/70 nm, respectively. The Cr film prevented the tungsten film from detaching from the Si substrate. The film was formed by standard radio-frequency magnetron sputtering. Ar was used as the sputtering gas. The base pressure of the sputtering chamber was 1×10^{-2} Pa and the sputtering pressure was 5×10^{-1} Pa. The deposition rate of tungsten was 13 nm/min. After deposition, we placed the samples in a vacuum furnace and annealed them by infrared heating. The base pressure of the furnace was 3×10^{-3} Pa. During the annealing process, we introduced O_2 gas. The gas flow rate was 1–1.5 SCCM (SCCM denotes cubic centimeter per minute at STP), and the total pressure of the furnace was $(4-6)\times10^{-2}$ Pa. A sample was annealed from room temperature up to 800 °C for 3 min, then maintained at 800 °C. After annealing, we cooled the furnace to room temperature

[a)]Author to whom correspondence should be addressed; Tel.: +81-3-5841-6362
[b)]Electronic mail: kojima@hnl.t.u-tokyo.ac.jp
[c)]Electronic mail: nagato@hnl.t.u-tokyo.ac.jp

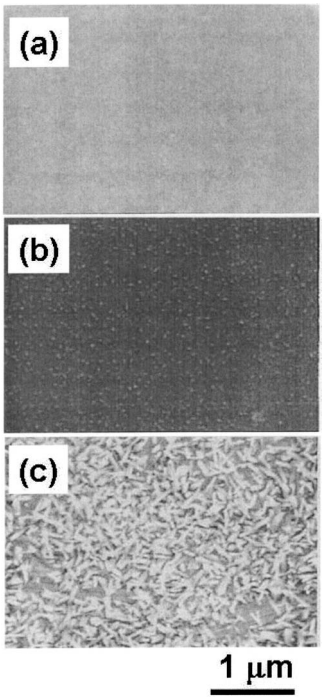

FIG. 1. SEM images of (a) nonannealed (sample A), (b) sample annealed from room temperature up to 800 °C, after which annealing was immediately stopped (sample B), and (c) sample annealed at 800 °C for 10 min (sample C).

for 15 min while maintaining O_2 gas flow, then removed the samples from the furnace. We prepared three different samples: a nonannealed sample (sample A); a sample that was annealed from room temperature up to 800 °C, after which annealing was immediately stopped (sample B); and a sample annealed at 800 °C for 10 min (sample C). Figures 1(a)–1(c) show surface images of samples A–C taken using scanning electron microscopes (SEM) (S-4000 and S-4160: Hitachi). Nanowires were not synthesized on sample A. Nanowires on sample B were very short. Nanowires were successfully grown on sample C. The samples were observed by TEM (JEM-2010F: JEOL) and analyzed by XRD (MXP3: McScience) with a Cu tube operated at 40 kV and 40 mA. For TEM observation, samples were protected by a Si wafer attached to the surface using thermosetting resin (G2: Gatan) and sliced using an Ar ion beam. The JEM-2010F was equipped with an energy-dispersive x-ray spectroscope (EDS), which was used to analyze the samples.

B. TEM observations and XRD analyses

Figure 2 shows (a) a cross-sectional TEM image of sample A and [(b) and (c)] EDS spectra taken from the points shown in the TEM image. The Mo peak originates from the TEM microgrid. The EDS spectra show that the upper black layer was W and the lower gray layer was Cr. No nanowires were observed on the W surface. Figure 3 shows (a) a cross-sectional TEM image of sample B and [(b) and (c)] EDS spectra taken from the points shown in the TEM image. The EDS spectra show that the lower black layer was W and the upper gray layer was tungsten oxide. The tungsten oxide layer was amorphous. The Cr and part of the W were removed by the Ar ion beam for the fabrication of the TEM sample. The thickness of the oxidized layer was 30 nm. Figure 4 shows a high-resolution (HR) TEM image of sample B. The nanowires were synthesized on the boundary between the oxidized layer and the W layer and were covered with a tungsten oxide layer. The lengths of the nanowires were less than 30 nm. Figure 5 shows a cross-sectional TEM image of sample C. The number of nanowires was greater than that on sample B, and the nanowires were longer than those on sample B. The amorphous layer on the surface was the resin used to protect the surface from the Ar ion beam. No oxidized layer was observed on sample B. The surface of the W layer was uneven and the nanowires were synthesized as a result of the surface unevenness.

Figure 6 shows a HRTEM image of a nanowire extracted from the substrate. The width of the nanowire was constant, and the nanowire had a uniform crystalline structure along the growth direction. The lattice spacing along the growth direction was determined to be 3.78 Å from the electron diffraction (ED) pattern. According to Ref. 34, the growth direction of the nanowire was identified to be that of monoclinic $W_{18}O_{49}(010)$.

Figure 7 shows XRD spectra of samples A–C. The XRD spectra indicate that sample A is a single β-W phase and sample C is a single α-W phase. This result shows that the original sputtered layer was β-W phase and turned into α-W

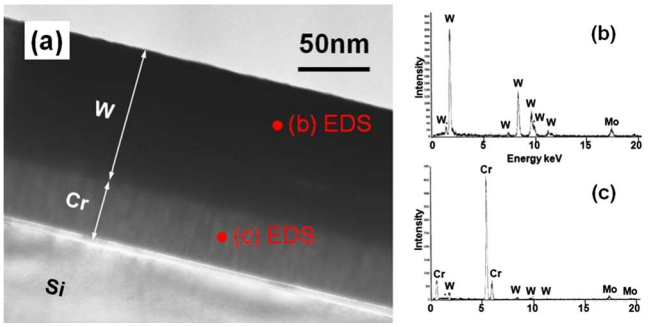

FIG. 2. (a) Cross-sectional TEM image of sample A and [(b) and (c)] EDS spectra taken from from the points shown in the TEM image.

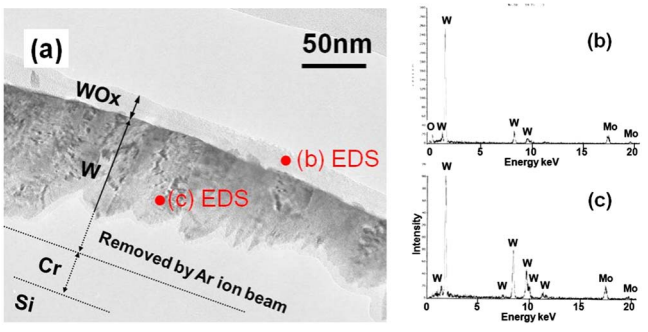

FIG. 3. (a) Cross-sectional TEM image of sample B and [(b) and (c)] EDS spectra taken from the points shown in the TEM image.

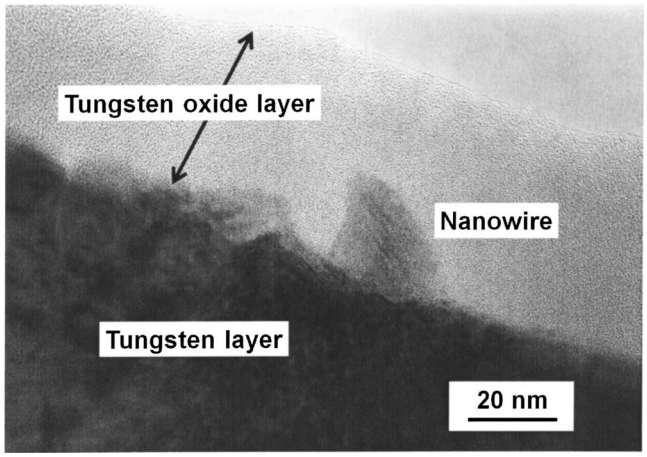

FIG. 4. High-resolution TEM image of surface of sample B.

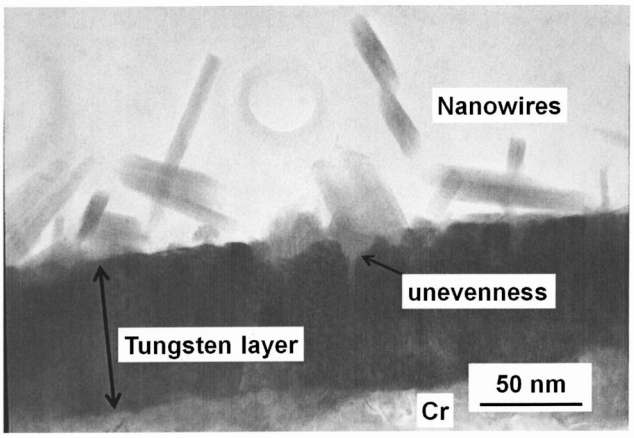

FIG. 5. Cross-sectional TEM image of sample C.

phase by annealing, as reported by Weerasekera *et al.*[35] The peak from sample B was between β-W (210) and α-W (110). This is because β-W was not completely transformed into α-W on sample B. The peak between β-W (210) and α-W (110) on a sample that has both β-W and α-W phases has been reported.[36] No peaks of tungsten oxide were confirmed because the amount of tungsten oxide was very small or it might be amorphous.

C. Proposal of growth model

We confirmed that the nanowires are synthesized on the boundary between the oxidized layer and the W layer by TEM observations. In this case, even if there are tungsten oxide molecules that evaporate from the W material, they cannot be absorbed on the nanowires because the nanowires are covered with an oxidized layer. Therefore, the solid-phase growth model is convincing as the growth mechanism of the nanowires.

In addition, based on TEM observations and XRD analyses, we propose the solid-phase growth model as follows (shown in Fig. 8). First, an amorphous oxidized layer is formed on the W surface by annealing in O_2. Second, nanowire nuclei are generated at irregular points on the W surface. Finally, tungsten oxide molecules migrate on the W surface into the nuclei, thus contributing to the nanowire growth.

III. VERIFICATION OF THE SOLID-PHASE GROWTH MODEL BY *EX SITU* EXPERIMENTS

A. Purpose of verification experiments

To verify the growth model suggested above, we must confirm two facts. The first is that the nanowire nuclei are generated at irregular points on the W surface. The possible causes of the irregular points on the surface are the phase transition from β-W to α-W during annealing and surface unevenness on the W surface. The second is that the oxidized layer migrates, which contributes to the nanowire growth. We confirm these two facts through some *ex situ* experiments.

B. Effect of phase transition of W on generation of nanowire nuclei

To investigate the effect of the phase transition of W on the synthesis of the nanowire nuclei, we examined whether the nanowires are synthesized on the W material with the α-W phase before nanowire growth.

We annealed a sputtered film, deposited under the same conditions as those given in Sec. II, at 800 °C for 10 min in a vacuum furnace without introducing O_2 gas. Figure 9 shows a (a) SEM image and (b) XRD spectrum of the sample after annealing. They indicate that the sample turned into α-W phase and that nanowires were not synthesized by annealing. We reannealed this sample at 800 °C for 10 min in the vacuum furnace while introducing O_2 gas. The base pressure and O_2 pressure of the vacuum furnace were the same as those given in Sec. II. After annealing, the furnace was cooled and the surface of the sample was observed by SEM.

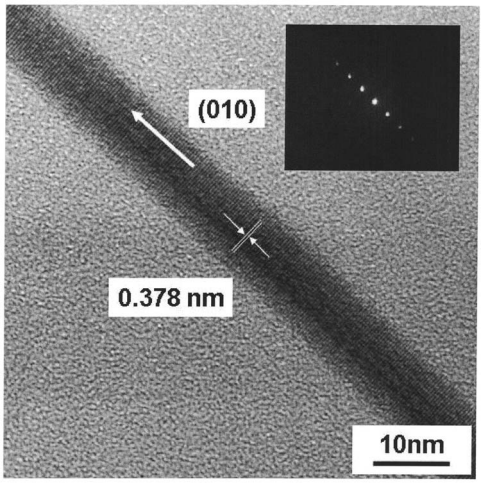

FIG. 6. TEM image of a synthesized nanowire.

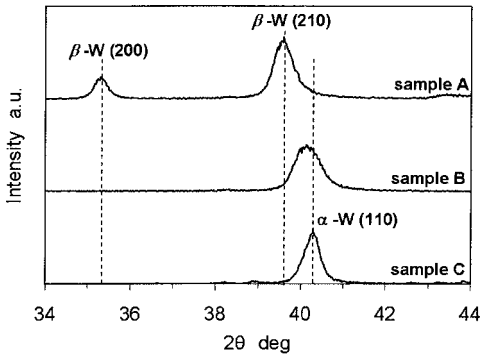

FIG. 7. XRD spectra of samples A–C.

Figure 10 shows a SEM image of the sample. We confirmed that nanowires were synthesized on the sample, which had the α-W phase before nanowire growth. This result indicates that the phase transition of W does not affect the generation of the nanowire nuclei.

C. Effect of surface unevenness of W surface on generation of nanowire nuclei

To investigate the effect of surface unevenness of the W surface on the generation of nanowire nuclei, we examined whether the nanowires are likely to be synthesized on the unevenness of the W surface fabricated artificially.

We used sputtered W/Cr films deposited under the same conditions as those given in Sec. II. Before the deposition of the W/Cr film, we fabricated holes on the Si wafer using a focused ion beam (FIB) (FB-2000A: Hitachi) to make holes on the W surface. Figure 11 shows an (a) atomic force microscope (AFM) image of a W surface and a cross-sectional image and (b) SEM image of the surface of the sputtered film. The size, depth, and pitch of the holes were 50×120, 30, and 200 nm, respectively. The sample was annealed at 800 °C for 10 min in the vacuum furnace while introducing O_2 gas. The base pressure and O_2 pressure were the same as those given in Sec. II. After annealing, the furnace was cooled and the surface of the sample was observed by SEM.

Figure 11(c) shows a SEM image of the sample after annealing. As shown in the image, some nanowires are synthesized from the holes on the surface. We investigated 203 nanowires and confirmed that 47% of nanowires were synthesized from the holes. Because the holes occupied only 15% of the surface, we can confirm that the nanowires are more likely to be generated from the holes. This result shows that the nanowire nuclei are generated as a result of the unevenness of the W surface.

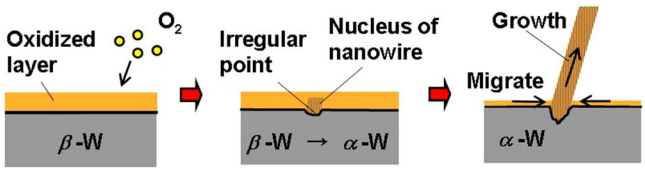

FIG. 8. Schematic of the solid-phase growth model proposed in this study.

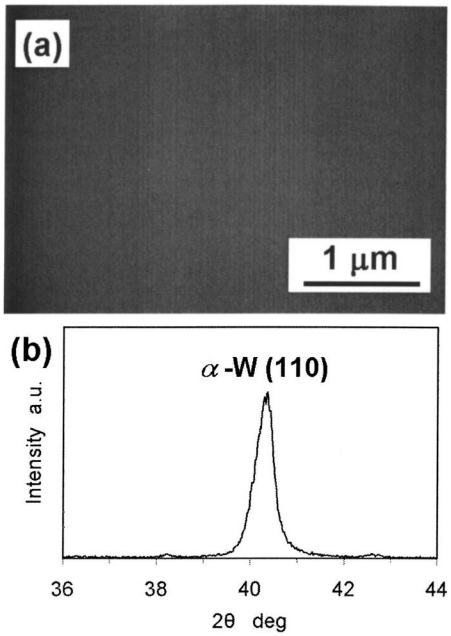

FIG. 9. (a) SEM image and (b) XRD spectrum of the sample annealed at 800 °C for 10 min without introducing O_2 gas.

D. Investigation of migration of tungsten oxide layer

To investigate whether the tungsten oxide layer migrates to contribute to the nanowire growth, we annealed a sputtered film with an amorphous tungsten oxide layer without introducing oxygen gas. If the nanowires grow after annealing, we can confirm that the tungsten oxide layer migrates, thus contributing to the nanowire growth, because the only tungsten oxide that can contribute to the nanowire growth is that in this oxidized layer after annealing.

We used sputtered W/Cr films deposited under the same conditions as those given in Sec. II. First, the samples were annealed from room temperature up to 800 °C while introducing O_2 gas, then annealing was immediately stopped (the same as for sample B in Sec. II). An oxidized layer similar to that shown in Fig. 3(a) was formed on the sample. After annealing, the furnace was cooled to room temperature and the samples were removed from the furnace. Then, the samples were reannealed without introducing O_2. The an-

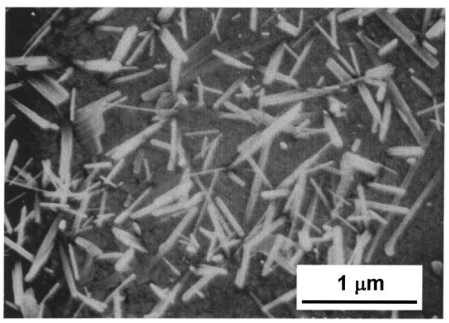

FIG. 10. SEM image of the sample annealed at 800 °C for 10 min without introducing O_2, then reannealed at 800 °C for 10 min while introducing O_2 gas.

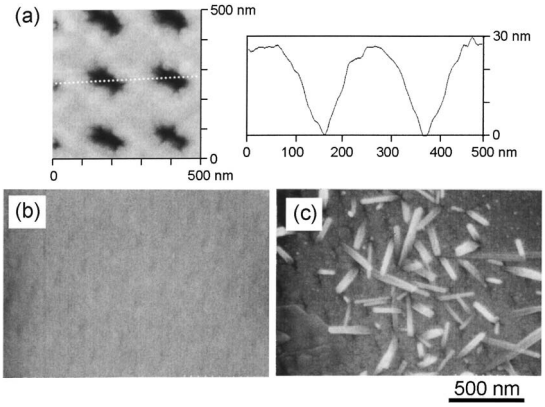

FIG. 11. (a) AFM image of surface and a cross-sectional image of the sputtered film on Si wafer processed using FIB. SEM images of the sputtered film on Si wafer processed using FIB (b) before annealing and (c) after annealing.

nealing temperatures were 750 and 800 °C. The annealing times were 3 and 10 min. The surface of the sample was observed by SEM after reannealing and compared with the sample before reannealing.

Figure 12 shows SEM images of (a) the sample before reannealing and the sample reannealed (b) at 750 °C for 3 min, (c) at 750 °C for 10 min, (d) at 800 °C for 3 min, and (e) at 800 °C for 10 min. By comparing Figs. 12(a) and 12(b), we can confirm that the nanowires grew by reannealing without O_2 gas. This result shows that tungsten oxide migrates on the surface to contribute to the growth of nanowires. On the other hand, the nanowires on the sample reannealed at 750 °C for 10 min and at 800 °C [Figs. 12(c)–12(e)] disappeared. This result shows that both the growth and sublimation of the nanowires occur during the annealing process.

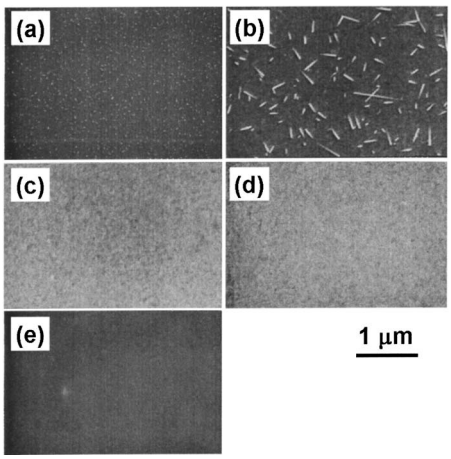

FIG. 12. SEM images of (a) sample before reannealing and samples reannealed (b) at 750 °C for 3 min, (c) at 750 °C for 10 min, (d) at 800 °C for 3 min, and (e) at 800 °C for 10 min.

TABLE I. Annealing temperatures of the tungsten material when the nanowires are synthesized on the tungsten material and on the substrate away from the tungsten material reported in various studies on the nanowires.

Synthesized on the tungsten material

Ref.	Author	Annealing temperature (°C)	W Material
3	F. Xu	1300	Wire
4	G. Y. Chen	650	Wire
9	H. Hashimoto	850–900	Filament
11	M. H. Cho	800–900	Sputtered film
12	C. H. Chen	700	Sputtered film
13	Y. Kojima	800	Sputtered film
21	V. K. Sarin	900	Powder
22	Y. Z. Jin	800	Powder
23	W. Sahle	900–1100	Powder
25	G. Gu	700	Tip
26	R. Seelaboyina	900	Tip
30	S. Jeon	700	CVD film
31	C. Klinke	900	Film
	This work	800	Sputtered film

Synthesized on the substrate away from tungsten material

Ref.	Author	Annealing temperature (°C)	W Material
1	Y.Q. Zhu	1600	Foil
2	Z. Liu	1600	Wire
5	K. Liu	1400	Filament
6	L.Chi	1150–1300	Filament
7	S. Vaddiraju	1500–2000	Filament
8	J. Thangala	1650	Filament
10	Y. B. Li	1000	Filament
16	K. Hong	650	Powder
17	A. Ponzoni	1400	Powder
18	Y. Baek	900–1100	Powder
19	C. C. Liao	950	Powder
20	K. Huang	1100	Powder
24	J. Zhou	1400	Powder

IV. DISCUSSION

From the results of the *ex situ* experiments, we confirmed two facts: the nanowire nuclei are generated at irregular points on the W surface, and the oxidized layer migrates to contribute to the nanowire growth. Therefore, we can conclude that the solid-phase growth model proposed above is convincing as the growth model of the nanowires synthesized on the sputtered tungsten films.

In addition to the growth model, we also confirmed that both the growth and sublimation of the nanowires occur during the annealing process. The nanowires grow when the growth rate is higher than the sublimation rate. On the other hand, when the sublimation rate is higher than the growth rate, the nanowires do not grow. The quantitative relation between the growth rate and the sublimation rate of the nanowires should be studied in the future.

Our group have reported that the number density of the nanowires increases as the oxidation degree of the sputtered tungsten films increases.[13] Using our growth model, we can explain this phenomenon as follows. With the increase in the oxidation degree, the amount of the oxidized layer that contributes to the nanowire growth increases. Thus, the number of nanowires whose growth rate exceeds the sublimation rate increases and more nanowires are synthesized.

As mentioned in the Introduction, other studies have reported that nanowires are synthesized on the substrate away from the tungsten material. Our proposed solid-phase growth model cannot explain this phenomenon. Table I shows the annealing temperature of the tungsten material when the nanowires are synthesized on the tungsten material and on the substrate away from the tungsten material reported in various studies on the nanowires. As shown in the table, the annealing temperature at which the nanowires are synthesized on the tungsten materials is likely to be lower than at which the nanowires are synthesized on the substrate away from the tungsten materials. Therefore, the solid-phase growth model proposed in this study can be applied to the nanowires that are synthesized on the tungsten material, and the growth mechanism of the nanowires that are synthesized on substrates away from the tungsten material is different from the growth model proposed in this study.

V. CONCLUSION

We have proposed a solid-phase growth model of tungsten oxide nanowires synthesized on sputtered tungsten films from the results of TEM observations, XRD analyses, and some *ex situ* experiments. The nanowire nuclei are generated at irregular points on the W surface. An amorphous oxidized layer is formed on the W surface by annealing, and tungsten oxide molecules migrate on the surface of W into nuclei, thus contributing to the nanowire growth.

ACKNOWLEDGMENTS

This work was supported by the assistance of Mr. Tsunakawa, Mr. Itoh, Mr. Ibe, and Mr. Fukawa of the University of Tokyo with the TEM images, EDS analyses, and XRD analyses. The authors would like to thank Professor Ikuhara and Dr. Shibata of the University of Tokyo for their helpful discussions.

[1] Y. Q. Zhu *et al.*, Chem. Phys. Lett. **20**, 327 (1999).
[2] Z. Liu, Y. Bando, and C. Tang, Chem. Phys. Lett. **372**, 179 (2003).
[3] F. Xu, S. D. Tse, J. F. Al-Sharab, and B. H. Kear, Appl. Phys. Lett. **88**, 243115 (2006).
[4] G. Y. Chen, V. Stolojan, D. C. Cox, C. Giusca, and S. R. P. Silva, *IEEE Conference on Emerging Technologies—Nanoelectronics—Proceedings* Vol. 376 (2006) (unpublished).
[5] K. Liu, D. T. Foord, and L. Scipioni, Nanotechnology **16**, 10 (2005).
[6] L. Chi, N. Xu, S. Deng, J. Chen, and J. She, Nanotechnology **17**, 5590 (2006).
[7] S. Vaddiraju, H. Chandrasekaran, and M. K. Sunkara, Nanotechnology **17**, 4830 (2006).
[8] J. Thangala, S. Vaddiraju, R. Bogale, R. Thurman, T. Powers, B. Deb, and M. K. Sunkara, Small **5**, 890 (2007).
[9] H. Hashimoto, K. Tanaka, and E. Yoda, J. Phys. Soc. Jpn. **15**, 1006 (1960).
[10] Y. B. Li, Y. Bando, D. Golberg, and K. Kurashima, Chem. Phys. Lett. **363**, 214 (2003).
[11] M. H. Cho *et al.*, J. Vac. Sci. Technol. B **22**, 1084 (2004).
[12] C. H. Chen *et al.*, Nanotechnology **17**, 217 (2006).
[13] Y. Kojima, K. Kasuya, T. Ooi, K. Nagato, K. Takayama, and M. Nakao, Jpn. J. Appl. Phys., Part 1 **46**, 6250 (2007).
[14] K. Nagato, Y. Kojima, K. Kasuya, H. Moritani, T. Hamaguchi, and M. Nakao, Appl. Phys. Express **1**, 014005 (2008).
[15] K. Kasuya, T. Ooi, Y. Kojima, and M. Nakao, Appl. Phys. Express **1**, 034005 (2008).
[16] K. Hong, M. Xie, and H. Wu, Nanotechnology **17**, 4830 (2006).
[17] A. Ponzoni *et al.*, Appl. Phys. Lett. **88**, 203101 (2006).
[18] Y. Baek and K. Yong, J. Phys. Chem. C **111**, 1213 (2007).
[19] C. C. Liao, F. R. Chen, and J. J. Kai, Sol. Energy Mater. Sol. Cells **90**, 1147 (2006).
[20] K. Huang, Q. Pan, F. Yang, S. Ni, and D. He, Physica E (Amsterdam) **39**, 219 (2007).
[21] V. K. Sarin, J. Mater. Sci. **10**, 593 (1975).
[22] Y. Z. Jin *et al.*, J. Phys. Chem. B **108**, 15572 (2004).
[23] W. Sahle, J. Solid State Chem. **45**, 324 (1982).
[24] J. Zhou *et al.*, Appl. Phys. Lett. **87**, 223108 (2005).
[25] G. Gu, B. Zheng, W. Q. Han, S. Roth, and J. Liu, Nano Lett. **2**, 849 (2002).
[26] R. Seelaboyina, J. Huang, J. Park, D. H. Kang, and W. B. Choi, Nanotechnology **17**, 4840 (2006).
[27] Y. B. Li, Y. Bando, and D. Golberg, Adv. Mater. (Weinheim, Ger.) **15**, 1294 (2003).
[28] Y. Baek, Y. Song, and K. Yong, Adv. Mater. (Weinheim, Ger.) **18**, 3105 (2006).
[29] J. Zhou, Y. Ding, S. Z. Deng, L. Gong, N. S. Xu, and Z. L. Wang, Adv. Mater. (Weinheim, Ger.) **17**, 2107 (2005).
[30] S. Jeon and K. Yong, Nanotechnology **16**, 1608 (2005).
[31] C. Klinke, J. B. Hannon, L. Gignac, K. Reuter, and P. Avouris, J. Phys. Chem. B **109**, 17787 (2005).
[32] J. Pfeifer, E. Badaljan, P. T. Buxbaum, T. Kovacs, O. Geszti, A. L. Toth, and H. J. Lunk, J. Cryst. Growth **169**, 727 (1996).
[33] W. Sahle and S. Berglund, J. Less-Common Met. **79**, 271 (1981).
[34] JCPDS Card No. 5-392 (unpublished).
[35] I. A. Weerasekera, S. I. Shah, D. V. Baxter, and K. M. Unruh, Appl. Phys. Lett. **64**, 3231 (1994).
[36] Y. G. Shen and Y. W. Mai, Mater. Sci. Eng., A **284**, 176 (2000).